16th World Conference on Earthquake, 16WCEE 2017

Santiago Chile, January 9th to 13th 2017

Paper N° 3794

Registration Code: S-L1460047189

INFLUENCE OF THREE HYSTERETIC MODELS ON THE INELASTIC DISPLACEMENT RESPONSE SPECTRA OF CONFINED MASONRY WALLS UNDER SEISMIC LOADING

J.J. Escobar (1), J.H. Chávez(2) and R. Pérez-Martínez*(2)

(1) Substitute professor. Civil Engineering, Instituto Tecnológico de La Paz, ITLP, B.C.S. México. E-mail: escomaj@hotmail.com
(2) Researcher, Faculty of Civil Engineering, Universidad Autónoma de Nuevo León (UANL), México, rho_p_m@yahoo.com
…

Abstract

In this article, the influence of three hysteretic models on the inelastic displacement response spectra of a confined masonry wall under seismic loading is evaluated. This study is done using ten strong-motion accelerograms taken from the SAC Phase 2 Steel Project that were recorded at Los Angeles area. For this purpose, the three types of behavior in hysteretic characteristics are: 1). Elasto-plastic model without degradation of strength and stiffness; 2). Hysteretic model with cyclic degradation of strength and stiffness; 3). Hysteretic model with cyclic degradation of strength and stiffness that takes into account the pinching phenomenon. In all cases, the differential equation of motion is solved by the Adams-Bashforth-Moulton method. From this study, it can be drawn some conclusions about the degree of refining the hysteretic model and its influence on the maximum inelastic displacement response spectra of a confined masonry panel. Results indicated that the degree of refining is not significant.

Keywords: Confined masonry walls; Hysteretic behavior; Maximum inelastic displacement.

1. Introduction

Performance-based seismic design philosophies have been applied to structural engineering, including masonry building, in the purpose to predict and evaluate analytically several levels of performances under seismic solicitations through the control of the peak lateral inelastic displacement demand [1]. Important part of this methodology consists in an appropriate mathematical idealization of nonlinear behavior of confined masonry walls subjected to reversed-cyclic lateral loads. Consequently, according to the progress in the knowledge of this physical phenomenon, there is a growing tendency to develop analytical hysteretic idealizations of higher degree of accuracy whose results are applied to study nonlinear seismic performance of a complete building by implementing specialized software that allows fitting the hysteretic rules, at the expense of a higher analytical processing demand. However, sometimes these refined hysteretic constitutive laws are not available in commercial analytical applications.

In this article, the influence of three hysteretic models on the inelastic displacement response spectra of confined masonry walls under seismic loading is evaluated. This study is done using ten strong-motion accelerograms taken from the SAC Phase 2 Steel Project which were recorded at Los Angeles area. The three types of behavior in hysteretic characteristics are: 1.) Elasto-plastic model without degradation of strength and stiffness; 2). Hysteretic model with cyclic degradation of strength and stiffness; 3). Hysteretic model with cyclic degradation of strength and stiffness that takes into account the pinching phenomenon. In all cases, the differential equation of motion is solved by the Adams-Bashforth-Moulton method. The results will provide insight into the appropriateness of applying and fitting hysteretic rules available in commercial software.

2. Experimental data of full-scale confined masonry wall

To assess the degree of analytical approximation of each hysteretic model, regarding to experimental results, it was selected the masonry wall M-1/4-E6, which is part of the experimental program of the National Center for Disaster Prevention of Mexico (CENAPRED) on full-scale confined masonry panels [2]. The masonry panel is composed of handmade clay solid bricks with horizontal reinforcement; as confining elements, external tie columns and bond beams of reinforced concrete are used (see Fig. 1). Reinforcement confinement details and joint mortar properties were defined in compliance with the requirements established by the 1993 issue of the Mexico City Building Code [3]. In Fig. 2 are shown the cyclic loading protocol and the hysteretic experimental response.

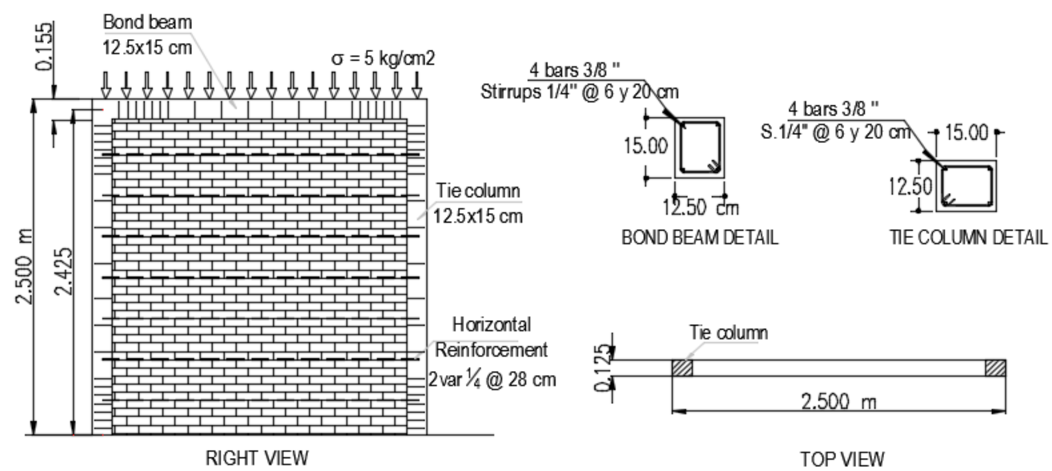

Fig. 1 – Characteristics of the full-scale wall specimen, M-1/4-E6.

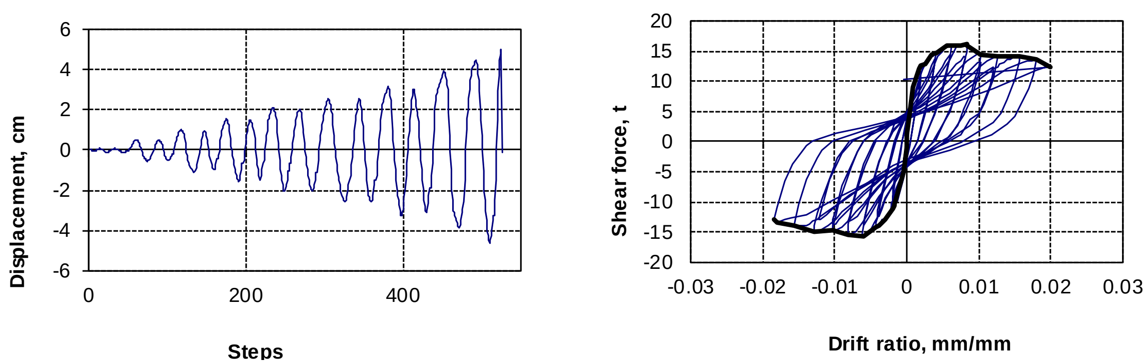

a) Cyclic loading protocol

b) Measured hysteretic response

Fig. 2 – Wall specimen M-1/4-E6: a) Cyclic loading protocol and b) Measured hysteretic response.

3. Hysteretic models

The choice of the three hysteretic models was based on a study of several works related to analytical modeling of the behavior of isolated masonry walls subjected to lateral loads, inferring that the most useful to achieve the stated purposes would be as follows: 1). Elasto-plastic model without degradation of strength and stiffness; 2). Hysteretic model with cyclic degradation of strength and stiffness [4]; 3). Hysteretic model with cyclic degradation of strength and stiffness that takes into account the pinching phenomenon [5]. The full description, step by step, of each one, is presented in reference [6]. In all cases, the hysteretic rules were implemented in the programming language, MATLAB R2012.

Table 1. Hysteretic models used in this study fitted to experimental data of full-scale confined masonry panel M-1/4-E6 tested in CENAPRED.

ID	Hysteretic behavior	Figure	Reference
fe	Elastic	- -	- -
f1	Elasto-plastic model without degradation of strength and stiffness	3a	- -
f2	Hysteretic model with cyclic degradation of strength and stiffness	3b	Flores (1995) [4]
f3	Hysteretic model with cyclic degradation of strength and stiffness that takes into account the pinching phenomenon	3c	Ruiz and Miranda (2003) [5]

3.1 Elastoplastic hysteretic model (function f_1)

The elasto-plastic model is the simplest and most commonly used hysteretic model, because it does not incorporate deterioration of strength and stiffness. During the loading stage, the system behavior is linear-elastic until the yield strength is reached. At yield, the stiffness switches from elastic stiffness to zero stiffness. During unloading stage, the stiffness is equal to the loading stiffness. Using the cyclic loading protocol of the wall, M-1/4-E6, the approach offered by this first model can be observed graphically in Fig. 3a, by superimposing the experimental and analytical responses.

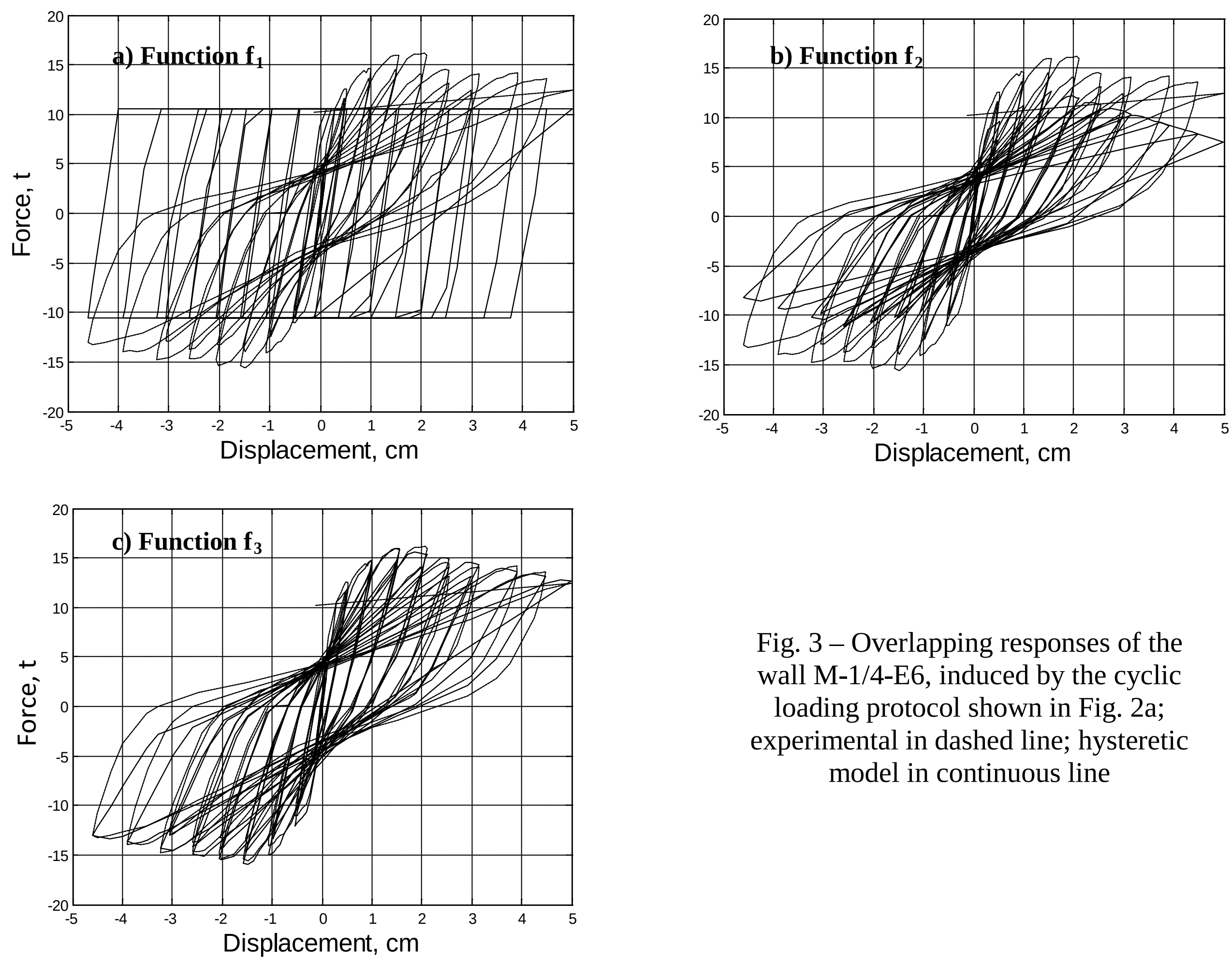

Fig. 3 – Overlapping responses of the wall M-1/4-E6, induced by the cyclic loading protocol shown in Fig. 2a; experimental in dashed line; hysteretic model in continuous line

3.2 Hysteretic model with cyclic degradation of strength and stiffness (function f_2)

This model is able to reproduce acceptably the hysteretic degradation of stiffness and strength by repeating the cyclic displacement; it is restricted to typical confined masonry walls based on handmade clay solid pieces and whose characteristics are representative to those used in low-cost Mexican housing. In the case of walls with other kind of masonry materials, an analogous behavior is estimated, but making the proper adjustments in the proposed expressions. Using the cyclic loading protocol of the wall, M-1/4-E6, the accuracy offered by this second model can be observed in Fig. 3b.

3.3 Hysteretic model with cyclic degradation of strength and stiffness that takes into account the pinching phenomenon with cyclic deterioration of strength and stiffness (function f_3)

This model can be considered of higher capability than the previous ones, because it takes into account aspects such as: stiffness degradation, cyclic strength degradation, which applies when there are repeated cyclic loads at the same displacement levels. Finally, the pinching behavior near the origin, which is characterized by large reductions in stiffness during reloading after unloading, along with stiffness recovery when displacement is imposed in the opposite direction. Using the cyclic loading protocol of the wall, M-1/4-E6, the accuracy offered by this third model can be observed in Fig. 3c.

4. Selection of seismic excitations

The set of time histories used for this research were recorded on a region of high seismic hazard belonging to Los Angeles area. After the Northridge earthquake, 1994, as part of the FEMA/SAC Steel Project, a set of time histories was developed for research purposes in the SAC Phase 2 Steel Project. The set of records can be considered representative of some other places with seismic activity, mainly due to soil conditions, magnitude, duration and frequency contents. In Table 2, it is shown a brief description of the 10 seismic events; considering its two orthogonal components resulting in a total of 20 accelerograms. This study employed the horizontal component of the higher acceleration of each event.

Table 2 – Set of characteristic seismic events taken from the SAC Phase 2 Steel Project, in bolt type are the strong-motion accelerograms used in this study (table continued on next page).

ID	Earthquake records	A	D_t	B	C
S_{1X}	Imperial Valley, 1940, El centro	6.9	0.02	39.38	452.03
S_{1Y}	**Imperial Valley, 1940, El centro**	**6.9**	**0.02**	**39.38**	**662.88**
S_{2X}	Imperial Valley, 1979, Array #05	6.5	0.01	39.38	386.04
S_{2Y}	**Imperial Valley, 1979, Array #05**	**6.5**	**0.01**	**39.38**	**478.65**
S_{3X}	**Imperial Valley, 1979, Array #06**	**6.5**	**0.01**	**39.08**	**295.69**
S_{3Y}	Imperial Valley, 1979, Array #06	6.5	0.01	39.08	230.08
S_{4X}	Landers, 1992, Barstow	7.3	0.02	79.98	412.98
S_{4Y}	**Landers, 1992, Barstow**	**7.3**	**0.02**	**79.98**	**417.49**
S_{5X}	**Landers, 1992, Yermo**	**7.3**	**0.02**	**79.98**	**509.70**
S_{5Y}	Landers, 1992, Yermo	7.3	0.02	79.98	353.35
S_{6X}	Loma Prieta, 1989, Gilroy	7	0.02	39.98	652.49
S_{6Y}	**Loma Prieta, 1989, Gilroy**	**7**	**0.02**	**39.98**	**950.93**

A= *Magnitude; Dt= Time resolution*; B= *Duration, s;* C= *PGA, cm/s²*

Table 2 – Set of characteristic seismic events taken from the SAC Phase 2 Steel Project, in bolt type are the strong-motion accelerograms used in this study (table continued from previous page).

ID	Earthquake records	A	D_t	B	C
S_{7X}	**Northridge, 1994, Newhall**	**6.7**	**0.02**	**59.98**	**664.93**
S_{7Y}	Northridge, 1994, Newhall	6.7	0.02	59.98	644.49
S_{8X}	Northridge, 1994, Rinaldi RS	6.7	0.005	14.945	523.30
S_{8Y}	**Northridge, 1994, Rinaldi RS**	**6.7**	**0.005**	**14.945**	**568.58**
S_{9X}	Northridge, 1994, Sylmar	6.7	0.02	59.98	558.43
S_{9Y}	**Northridge, 1994, Sylmar**	**6.7**	**0.02**	**59.98**	**801.44**
S_{10X}	**North Palm Spring, 1986**	**6**	**0.02**	**59.98**	**999.43**
S_{10Y}	North Palm Spring, 1986	6	0.02	59.98	967.61

A= *Magnitude; Dt= Time resolution*; B= *Duration, s;* C= *PGA, cm/s^2*

The time resolution, D_t, of each accelerogram is: 0.005, 0.01 y 0.02 seconds. To take faithfully all numerical information representative of the physical properties of earthquakes, in the process involving the definition of the step size in the solution of the numerical method used, the value D_t was established as an upper limit; another upper limit is assigned according to the criteria of the numerical method. The frequency content of each earthquake was studied by applying a Fourier spectral analysis. Subsequently, applying the index known as the Nyquist frequency, it was determined that there is no frequency content above 25 Hz, for most accelerograms with Dt =0.02 s, and none above 100 Hz for, Dt =0.005 s [7].

5. Dynamic system properties.

The dynamic single degree of freedom system (Fig. 4) is represented by the differential equation (ED) of motion described in Eq. (1), and solved by the predictor corrector method, Adams-Bashforth-Moulton. The mass remains constant with, m=0.01 ton/(cm/s^2), and damping of ε=2%. The value of, c, is assigned depending on the natural period T, as follow: f= 2π/T, c= ε (2*m*f). The spring stiffness is replaced by the hysteretic properties of each function (f_e, f_1, f_2, & f_3) and; in all cases, the initial elastic stiffness is assigned depending on the natural period as, K= m*(2 π / T)^2. The step size for the numerical method remained constant for all functions with, AM=0.001 y A_{tm}=0.002.

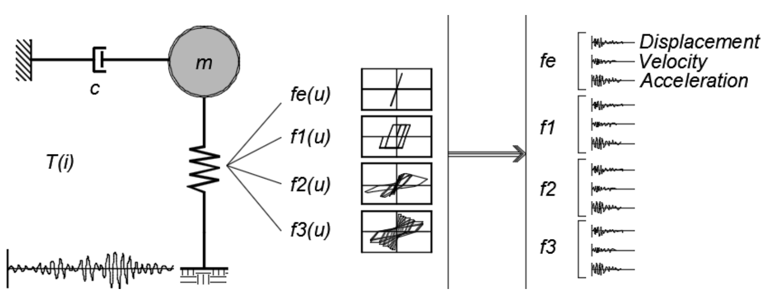

Fig. 4 – Scheme of the single degree of freedom system and its response.

Differential equation of dynamic equilibrium for a single horizontal degree of freedom system:

$$m\ddot{u} + c\dot{u} + f(u) = -m\,s_0 \tag{1}$$

Where m: mass of the system; c: damping coefficient; ü, u, u: acceleration, velocity, and relative displacement, respectively; f(u) is the restoring force of the system provided by the functions; and s_0 the ground acceleration.

The numerical process consisted in setting a value for the natural period T; the properties *m*, ε and *c* remain constant; the spring stiffness is replaced by each hysteretic function; subsequently, a seismic record was evaluated and a response in time for displacement, velocity, and acceleration were estimated. The peak in absolute value of each response is chosen, and represents a point on the graph of the response spectrum.

2.4.2 Calibration of hysteretic models.

For the proper functioning of hysteretic models, within the numerical method, it was necessary to calibrate the parameters in some models according to the change of natural period T. After that, each increase meant a decrease of the initial elastic stiffness K, and consequently, without the proper settings, the results estimated by the numerical method were inadequate due to a numerical destabilization.

fe: In the case of the elastic function, no adjustment was necessary. The elastic stiffness value was varying according to the period value $K = m^*(2\pi / T)^2$, thus upper envelope limits are no required.

f_1: In the elastoplastic function, a shear force of 10.5 t was assigned to the backbone curve that corresponds to point VR_{DF}, analytically estimated according to Mexican code [8]. In fact, the application of this model is no complicated. The initial elastic stiffness is used in the same way as in the function fe.

f_2: In the function with stiffness degradation, Table 3 presents the points used to build the backbone curve at each increment of the period defined. To carry out the fitting, first, the value for D3 was defined from the last displacement reached with the elastic function fe, which gave us valuable information to know what could be expected when more elaborate functions were applied. Subsequently, the points D2, like the forces, F1, F2 and F3 were fitted such that the original shape, proposed for the wall M-1/4-E6 was preserved, ensuring that slope changes are minors to the initial ones. In Fig. 5, it is shows the shape of the envelope curve as function of period T; the initial stiffness is in function of the period, and the point D1 can be derived by defining F1.

Table 3 – Setting parameters in envelope curves using function f_2.

T	K	D1 cm	D2 cm	D3 cm	F1 t	F2 t	F3 t
0.1	39.47842	0.2660	0.718	1.488	10.50	12.60	10.08
0.2	9.869604	1.0639	1.965	3.500	10.50	12.60	10.08
0.3	4.386491	2.3937	3.173	4.500	10.50	12.60	10.08
0.4	2.467401	4.2555	5.826	8.500	10.50	12.60	10.08
0.5	1.579137	6.6492	9.184	13.500	10.50	12.60	10.08
0.6	1.096623	9.5749	15.282	25.000	10.50	12.60	10.08

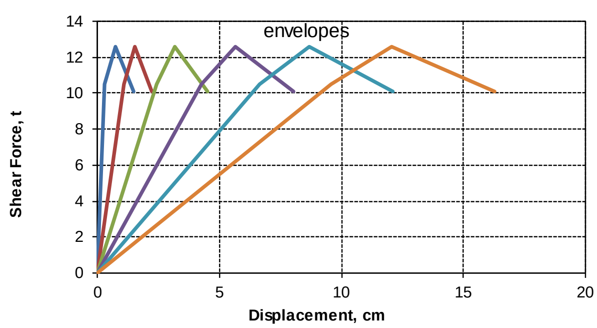

Fig. 5 – Backbone curves using setting parameters of function f_2.

On the other hand, it was also necessary to calibrate the parameters that define the slopes of the loading and unloading hysteretic branches, ensuring minors slopes than the initial K. A reasonable performance is observed when force-deformation response is plotted and the path of the hysteretic loops, within the limits imposed by the backbone curve, is verified. After a value of T > 0.6 s, the hysteretic rules have a misbehavior so this value was imposed as maximum. The fitted parameters of function f_2 are shown in Table 4.

Table 4 – Setting parameters of the loading and unloading branches when function f_2 is used.

T	K	Loading		Unloading	
		a	b	a	b
0.1	39.47842	100,000,000	300	10,000,000	100
0.2	9.869604	100,000,000	100	70,000,000	12
0.3	4.386491	10,000,000	8	1,000,000	3
0.4	2.467401	1,000,000	5	200,000	2
0.5	1.579137	90,000	3	10000	1
0.6	1.096623	10,000	4	1,000	1

f_3: In the case of the function with stiffness degradation and cyclic strength degradation, it is applied the same criterion for function f_2. In Tables 5, 6 and Fig. 6, the parameters fitted for function f_3 are presented as function of period T, and the shape of theirs backbone curves, respectively.

Table 5 – Setting parameters in envelope curves using function f_3.

T	K	D1	D2	D3	D4	F1	F2	F3	F4
		cm	cm	cm	cm	t	t	t	t
0.1	39.47842	0.27	1.02	1.77	4.02	10.50	12.60	13.13	11.55
0.2	9.869604	1.06	2.31	3.56	6.06	10.50	12.60	13.13	11.55
0.3	4.386491	2.39	3.64	6.14	8.64	10.50	12.60	13.13	11.55
0.4	2.467401	4.26	5.51	8.01	11.76	10.50	12.60	13.13	11.55
0.5	1.579137	6.65	9.15	11.65	14.15	10.50	12.60	13.13	11.55
0.6	1.096623	9.57	12.07	14.57	17.07	10.50	12.60	13.13	11.55

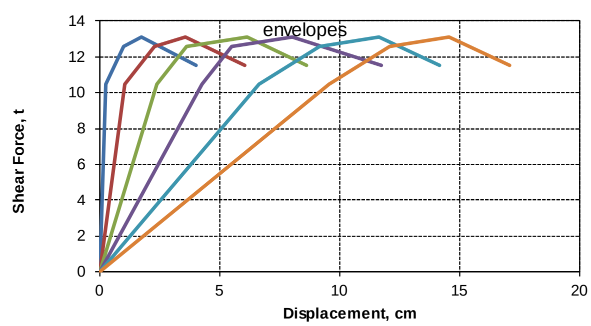

Fig. 6 – Backbone curves using setting parameters of function f_3.

Table 6 – Setting parameters of the loading and unloading branches when function f_3 is used.

T	K	HC	HBD	HBE	HS	LDA	ETA	MIU
0.1	39.47842	3	0.01	0.01	0.015	0.025	5	6.64
0.2	9.869604	5	0.01	0.01	0.015	0.03	5	3.35
0.3	4.386491	30	0.01	0.01	0.015	0.03	5	2.57
0.4	2.467401	30	0.01	0.01	0.015	0.03	5	1.88
0.5	1.579137	30	0.01	0.01	0.015	0.03	5	1.75
0.6	1.096623	30	0.01	0.01	0.015	0.03	5	1.52

6. Results

After analyzing the confined masonry panel M-1/4-E6 modeled with the four hysteretic models of Table 1 under the influence of the ten strong-motion accelerograms of Table 2, there were obtained the acceleration response spectra and displacement response spectra for each earthquake which plots are presented in Figs. 7 – 16.

For example, in Figs. 7a and 7b are presented the acceleration response spectra and displacement response spectra, respectively, under component S_{1Y} of Imperial Valley earthquake, 1940. Additional results and details about the methodology and the coefficients used in this study are presented by Escobar (2015) [6].

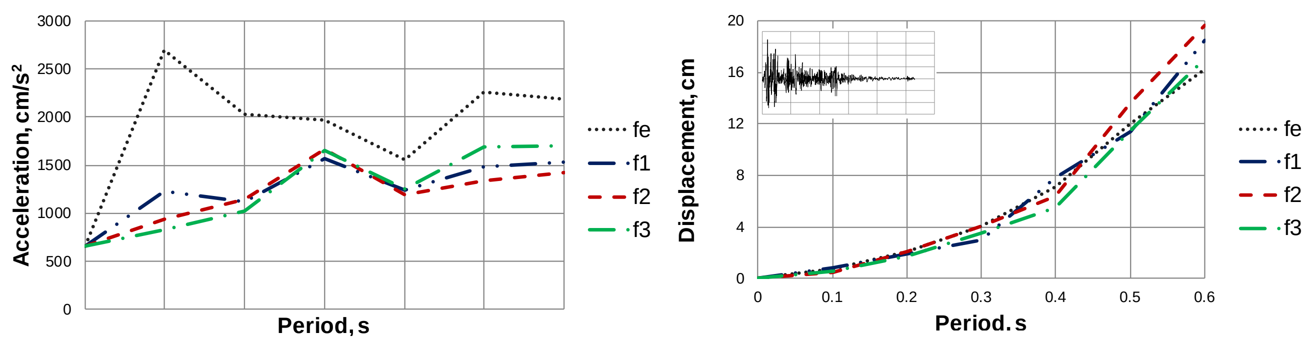

a) Acceleration response spectra

b) Displacement response spectra

Fig. 7 – Imperia Valley earthquake, 1940; component S_{1Y}

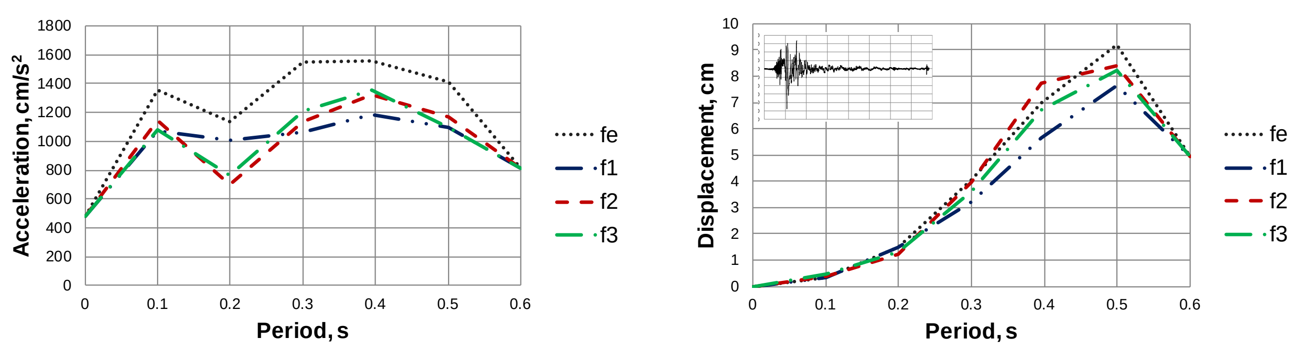

a) Acceleration response spectra

b) Displacement response spectra

Fig. 8 – Imperial Valley earthquake, 1979; component S_{2Y}

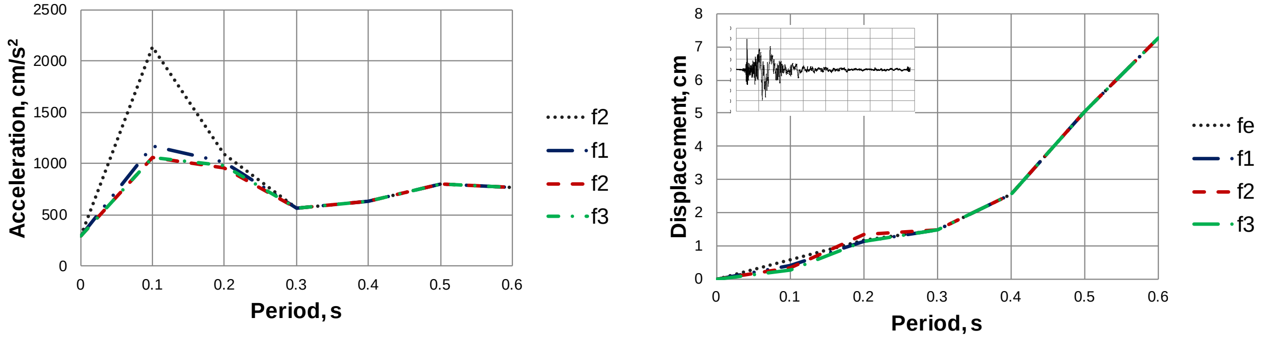

a) Acceleration response spectra b) Displacement response spectra

Fig. 9 – Imperial Valley earthquake, 1979; component S_{3X}

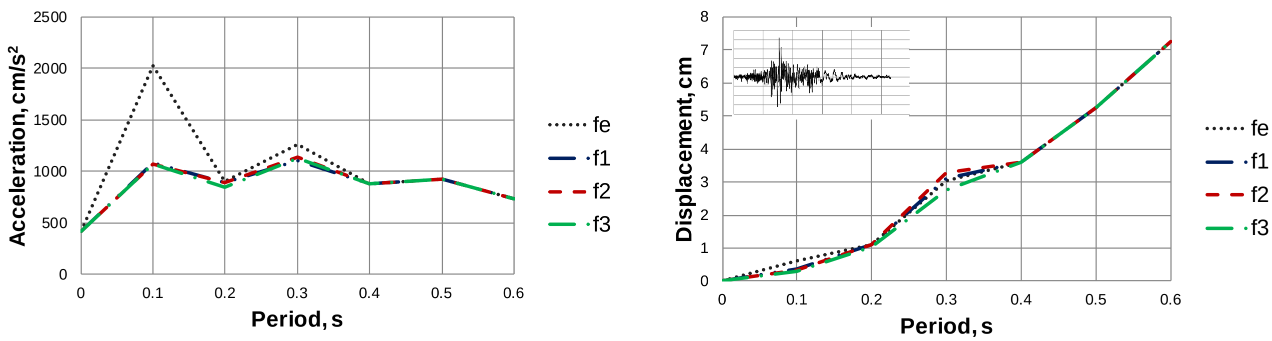

a) Acceleration response spectra b) Displacement response spectra

Fig. 10 – Landers earthquake, 1992; component S_{4Y}

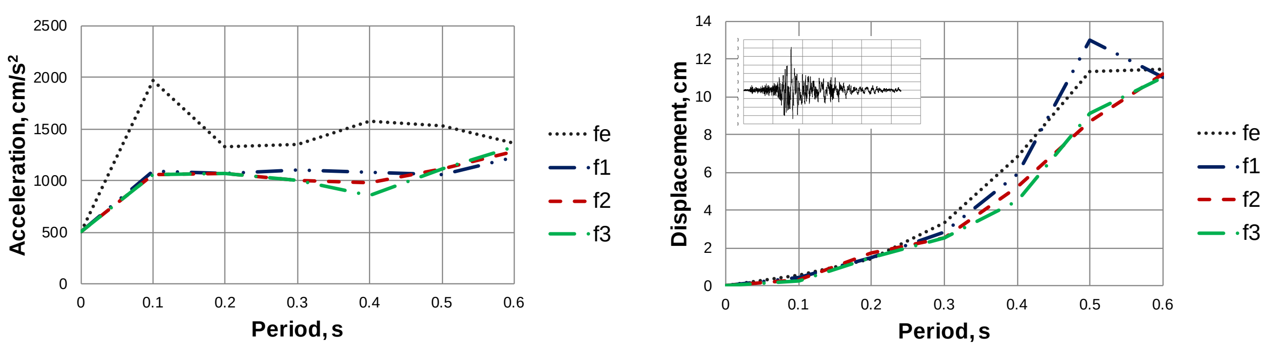

a) Acceleration response spectra b) Displacement response spectra

Fig. 11 – Landers earthquake, 1992; component S_{5X}

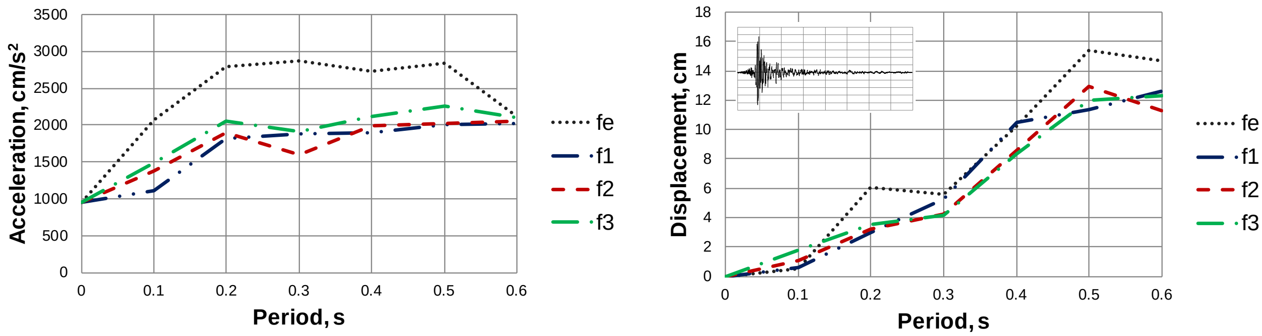

a) Acceleration response spectra b) Displacement response spectra

Fig. 12 – Loma Prieta earthquake, 1989; component S_{6Y}

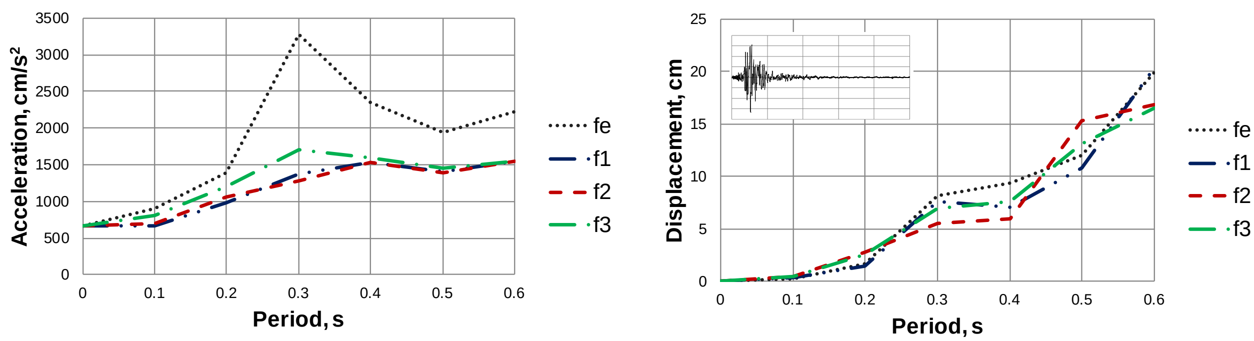

a) Acceleration response spectra b) Displacement response spectra

Fig. 13 – Northridge earthquake, 1984; component S_{7Y}

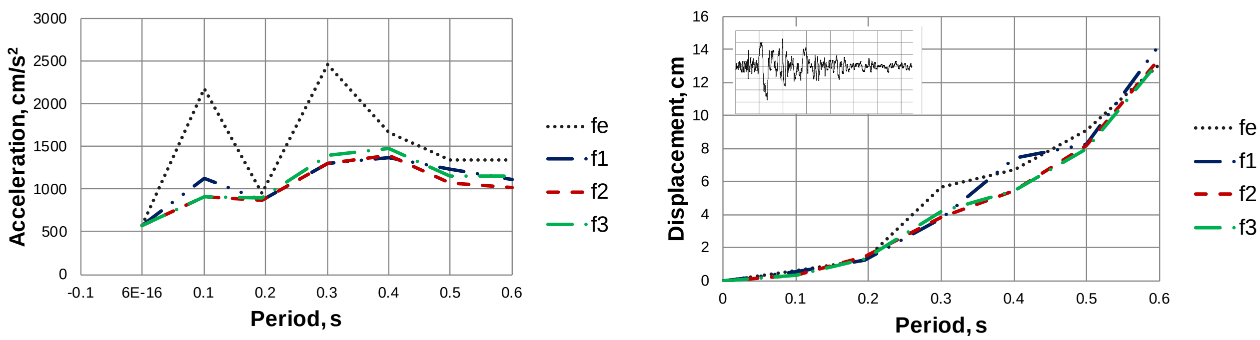

a) Acceleration response spectra b) Displacement response spectra

Fig. 14 – Northridge earthquake, 1994; component S_{8Y}

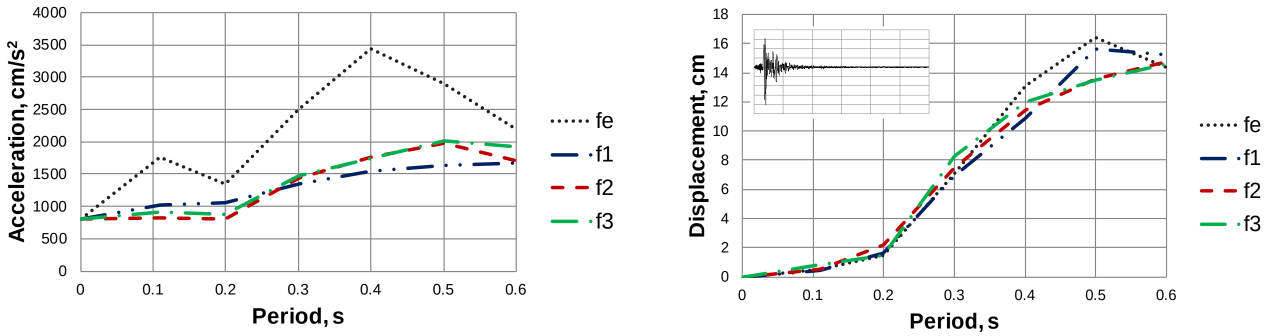

a) Acceleration response spectra b) Displacement response spectra

Fig. 15 – Northridge earthquake, 1994; component S_{9Y}

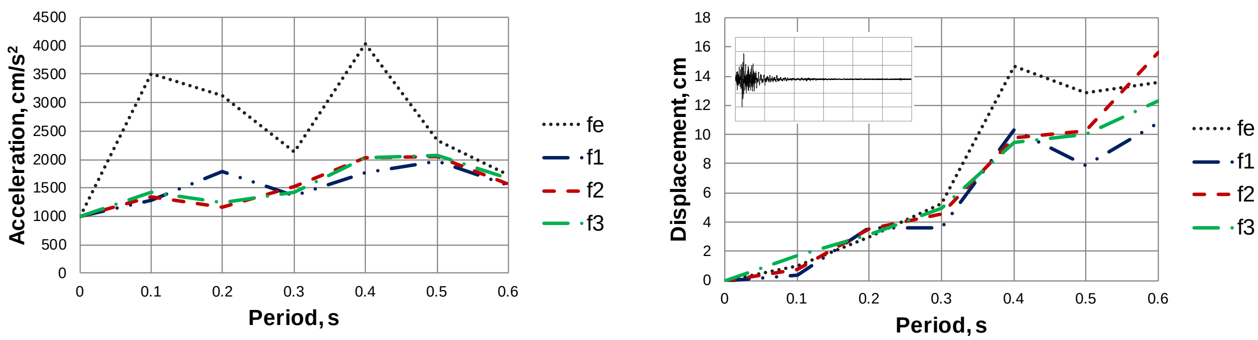

a) Acceleration response spectra b) Displacement response spectra

Fig. 16 – North Palm Spring earthquake, 1986; component S_{10X}

7. Conclusion

The influence of three hysteretic models on the inelastic displacement response spectra of the confined masonry wall M-1/4-E6 under seismic loading is a practical and direct study where results are clearly exposed in Figs. 7b – 16b. Thus, based on the process and obtained results, the next observations and conclusions are made:

1) Zones of overlapping with curve of the function fe shows that the inelastic level of the functions f_1, f_2, & f_3 was not reached; It could be related to low soil accelerations in combination with the constant value of mass.

2) The points that show a difference in ordinate value are directly affected by the stiffness degradation provided by the ascending and undescending branches of the hysteretic functions; thus, the influence of functions, in determining the peak displacement, is in the way of idealizing stiffness degradation.

3) In general terms, even when the response for displacement differs in the time domain for each function, a similarity is observed in each peak response as shown in the curve shapes of displacement response spectra, mainly due to the envelop curves of each hysteretic function are close in magnitude and the forces induced by the earthquakes are limited in the dynamic structural system. Thus, due to its minimum analytical processing, the elasto-plastic function f_1 can be acceptably employed in preliminary studies; subsequently, functions, f_2, or f_3, must be used for the final design phase of a short period structural system. This implies an easy adaptation in the commercial software with nonlinear scope of analysis.

8. Acknowledgements

The first author acknowledges the support given by Faculty of Civil Engineering, Autonomous University of Nuevo Leon (UANL). The authors express his gratitude to the Mexican Ministry of Education for the financial support to present this paper.

9. Copyrights

10. References

[1] Terán A, Zúñiga O (2007): Evaluación estructural basada en desplazamientos para edificaciones de mampostería confinada, el desarrollo mexicano. *V Simposio Nacional de Ingeniería Estructural en la Vivienda (SMIE)*, Querétaro, México.

[2] Aguilar, G., Meli, R., Díaz, R., and Vázquez-del-Mercado, R. (1996): Influence of Horizontal Reinforcement on the Behavior of Confined Masonry Walls, *Proc. of the 11th World Conference on Earthquake Engineering*, Paper No. 1380, Acapulco, Mexico.

[3] MCBC (1993): Reglamento de Construcciones del Distrito Federal (México City Building Code). *Gaceta Oficial del Departamento del Distrito Federal*, México DF (in Spanish).

[4] Flores LE (1995): Estudio analítico de estructuras de mampostería confinada. B.Sc. Thesis, *National Autonomous University of Mexico (UNAM)*, 106.

[5] Ruiz J, Miranda E (2003): Evaluación de los factores de reducción de resistencia por ductilidad para estructuras de mampostería cimentadas en terreno firme. *Revista de Ingeniería Sísmica (SMIS)*, ***69***, *1-23*.

[6] Escobar JJ (2015): Efecto sísmico de tres modelos histeréticos para muros de mampostería confinada en los espectros de respuesta inelásticos. M.Sc. Thesis, *Autonomous University of Nuevo Leon (UANL)*, 156.

[7] Chavez JH (2009): Non linear torsional behavior of buildings under earthquake ground motion. Ph. D. Thesis, *Illinois Institute of Technology*; Chicago, Illinois. December.

[8] MCBC (2004). Reglamento de Construcciones del Distrito Federal (Mexico City Building Code), *Gaceta Oficial del Departamento del Distrito Federal*, México DF (in Spanish)